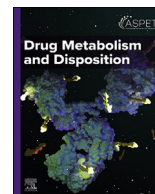




Drug Metabolism and Disposition




journal homepage: www.dmd.aspetjournals.org



SPECIAL SECTION: SEX AND HORMONAL INFLUENCES ON DRUG METABOLISM AND DISPOSITION, AND RELATED STUDIES—ARTICLE

Sex-dependent alterations in cardiac cytochrome P450-mediated arachidonic acid metabolism in pressure overload–induced cardiac hypertrophy in rats



Samar H. Gerges ¹ , Sara A. Helal ^{1,2}, Heidi L. Silver ³ , Jason R.B. Dyck ³,
Ayman O.S. El-Kadi ^{1,*} 

¹ Faculty of Pharmacy and Pharmaceutical Sciences, University of Alberta, Edmonton, Alberta, Canada

² Department of Biochemistry, Faculty of Pharmacy, Tanta University, Tanta, Egypt

³ Department of Pediatrics, Faculty of Medicine and Dentistry, University of Alberta, Edmonton, Alberta, Canada

ARTICLE INFO

Article history:

Received 23 January 2025

Accepted 25 March 2025

Available online 31 March 2025

Key words:

Arachidonic acid

Cardiac hypertrophy

Cytochrome P450

Epoxyeicosatrienoic acids

Hydroxyeicosatetraenoic acids


ABSTRACT

Cardiac hypertrophy is a risk factor for heart failure and is usually less common in young women than in men. Cytochrome P450 (CYP) enzymes in the heart metabolize arachidonic acid into hydroxyeicosatetraenoic acids (HETEs), which generally have hypertrophic effects, and epoxyeicosatrienoic acids, which have cardioprotective effects. In this study, we aimed to investigate sex-specific differences in cardiac hypertrophy and cardiac CYP, HETE, and epoxyeicosatrienoic acid levels in response to pressure overload. Adult male and female Sprague–Dawley rats were subject to sham or abdominal aortic constriction (AAC) surgeries. Five weeks postsurgery, cardiac function was assessed by echocardiography. The mRNA and protein levels of hypertrophic markers and CYP enzymes were measured by real-time polymerase chain reaction and Western blot. Heart tissue HETE levels and microsomal formation of HETEs and epoxyeicosatrienoic acids were measured by liquid chromatography–tandem mass spectrometry. Our results show significant sex-specific differences in AAC-induced cardiac hypertrophy. Echocardiography and ventricular wall measurements showed more hypertrophy in male rats. Some hypertrophic markers were significantly upregulated only in male AAC rats and were significantly higher in the hearts of male rats compared to female AAC rats. Different CYP hydroxylases such as CYP1B1, CYP4A, and CYP4F and epoxigenases such as CYP2C and CYP2J10 were significantly upregulated in the hearts of male AAC rats only. The heart level of 12(R)-HETE and the microsomal formation of several HETEs were also significantly increased only in male rats. In conclusion, male rats developed stronger AAC-induced cardiac hypertrophy compared to female rats, which was accompanied by a significant increase in cardiac CYP enzymes and HETEs.

Significance statement: Previous studies demonstrated that male rats experience more severe cardiac hypertrophy compared to female rats. To our knowledge, this research is the first to investigate and compare the expression of cytochrome P450 enzymes and arachidonic acid metabolites in male and female rat hearts following pressure overload–induced hypertrophy. This study highlights significant sex-specific differences in cytochrome P450-mediated metabolism during hypertrophy, providing valuable insights into the molecular mechanisms underlying these responses and identifying potential targets for sex-specific therapies in cardiac diseases.

© 2025 The Author(s). Published by Elsevier Inc. on behalf of American Society for Pharmacology and Experimental Therapeutics. This is an open access article under the CC BY-NC-ND license (<http://creativecommons.org/licenses/by-nc-nd/4.0/>).

* Address correspondence to: Dr Ayman O.S. El-Kadi, Faculty of Pharmacy & Pharmaceutical Sciences, 2142J Katz Group-Rexall Centre for Pharmacy and Health Research, University of Alberta, Edmonton, Alberta, Canada T6G 2E1. E-mail: aekadi@ualberta.ca

 This article has supplemental material available at dmd.aspetjournals.org.

1. Introduction

Cardiac hypertrophy is an enlargement of the heart muscle in response to different stimuli. Pathological hypertrophy occurs in response to insults such as hemodynamic overload and myocardial injury and could lead to serious conditions such as heart failure and potentially death (Shimizu and Minamino, 2016). The early stage of pathological hypertrophy is known as compensated hypertrophy because the heart is capable of compensating for the elevated stress by increasing in size while maintaining normal cardiac function. However, persistent hypertrophy could eventually lead to fibrosis and decompensation, characterized by a decrease in the systolic function and progression to heart failure (Nakamura and Sadoshima, 2018). Heart failure affects nearly 64 million people worldwide (Shahim et al, 2023). Approximately 750,000 Canadians are currently living with heart failure, and it is estimated to cost more than \$2.8 billion per year by 2030 (Tran et al, 2016).

Cytochrome P450 (CYP) is a superfamily of enzymes that mediate the oxidative metabolism of exogenous and endogenous molecules. Several CYP enzymes are expressed in the human heart (Chaudhary et al, 2009; Jenkins et al, 2009). Cardiac CYP enzymes metabolize arachidonic acid (AA) into different metabolites that play an important role in cardiovascular health (Elbekai and El-Kadi, 2006; Zordoky et al, 2008; El-Sherbeni and El-Kadi, 2014; Althurwi et al, 2015; Gerges and El-Kadi, 2022). CYP hydroxylases such as CYP1A1, CYP1B1, CYP2E1, CYP4A, and CYP4F produce hydroxyeicosatetraenoic acids (HETEs); and CYP epoxygenases such as CYP2B, CYP2C, and CYP2J produce epoxyeicosatrienoic acids (EETs). HETEs are classified into midchain (5-, 8-, 9-, 11-, 12-, 15-HETE), subterminal (16-, 17-, 18-, 19-HETE), and terminal (20-HETE) HETEs, all of which, except for 20-HETE, exist as R and S enantiomers. In addition, there are 4 regioisomeric EETs (5,6-EET; 8,9-EET; 11,12-EET; and 14,15-EET), which exist as S/R and R/S enantiomers (Elbekai and El-Kadi, 2006; El-Sherbeni and El-Kadi, 2017). EETs are metabolized by soluble epoxide hydrolase (sEH) into less active metabolites (Spector, 2009). CYP hydroxylases, especially CYP1B1 and its associated midchain HETEs, were found to be significantly elevated in different cardiac hypertrophy models, and their inhibition was associated with the amelioration of hypertrophy (El-Sherbeni and El-Kadi, 2014; Maayah et al, 2016, 2017, 2018; Maayah and El-Kadi, 2016b; Elkhatali et al, 2017; Shoieb and El-Kadi, 2018,2020; Pascale et al, 2021; Shoieb et al, 2022). In contrast, EETs have cardioprotective and anti-hypertrophic effects (Lai and Chen, 2021; Zhang et al, 2022). Treatment for cardiomyocytes with HETEs resulted in the induction of hypertrophy (Maayah et al, 2015; Maayah and El-Kadi, 2016a; Hidayat et al, 2023; Isse et al, 2023b; Helal et al, 2024), whereas 14,15-EET demonstrated antihypertrophic effects (Tse et al, 2013).

Evidence from experimental and clinical studies indicates significant sex-specific differences in the pathogenesis of different cardiovascular diseases (CVDs) (Mosca et al, 2011; Regitz-Zagrosek and Kararigas, 2017; Kessler et al, 2019; Gerges and El-Kadi, 2022). The mechanisms underlying the apparent female sex protection are not yet fully elucidated, but they are largely attributed to the cardioprotective effects of estrogen (dos Santos et al, 2014). Differences in the eicosanoid formation and metabolism pathways between males and females could also be an important player in the sexual dimorphism observed in CVDs (Gerges and El-Kadi, 2022, 2023). We have previously found significant differences between male and female rats in the cardiac levels of CYP enzymes and HETEs (Gerges and El-Kadi, 2023). In this study, we aimed to investigate sex-specific differences in pressure overload-induced cardiac hypertrophy in rats and the associated changes in cardiac CYP enzymes, HETEs, and EETs.

2. Material and methods

2.1. Chemicals

The TRIzol reagent used for mRNA extraction was Invitrogen brand (Thermo Fisher Scientific). High-Capacity cDNA Reverse Transcription Kit and SYBR Green polymerase chain reaction (polymerase chain reaction [PCR]) Master Mix were purchased from Applied Biosystems. Real-time PCR primers were formulated by and purchased from Integrated DNA Technologies. Trans-Blot Turbo RTA Transfer Kit and 2X Laemmli Sample Buffer were purchased from Bio-Rad Laboratories. CYP1A2 (sc-53241) and CYP4A1 (sc-53248) mouse monoclonal primary antibodies were purchased from Santa Cruz Biotechnology; CY4F2 rabbit polyclonal primary antibody (ab230709) and glyceraldehyde-3-phosphate dehydrogenase mouse monoclonal antibody (ab8245) were purchased from Abcam; CYP1B1 rabbit polyclonal primary antibody (PA5-28040) was purchased from Invitrogen (Thermo Fisher Scientific); and CYP2J rabbit polyclonal primary antibody (ABS1605) was purchased from MilliporeSigma. Enhanced chemiluminescence Western blotting detection reagents were obtained from Cytiva.

The standard (\pm) 5-, 8-, 9-, 11-, 12-, 15-, 16-, 17-, 18-, 19-, and 20-HETE, as well as 5,6-; 8,9-; 11,12-; and 14,15-EET, and the internal standards 20-HETE-D6 and 11,12-EET-D11 were obtained from Cayman Chemical. Isopropyl alcohol, ethyl acetate, and glacial acetic acid were purchased from Sigma Aldrich. Acetonitrile, methanol, magnesium chloride hexahydrate, potassium phosphate dibasic, and potassium phosphate monobasic were purchased from MilliporeSigma. High-performance liquid chromatography water was obtained from Fisher Scientific Co. All other chemicals used were obtained from Sigma Aldrich.

2.2. Animals

All procedures involving experimental animals were performed in accordance with the Animal Research: Reporting of In Vivo Experiments guidelines and the Guide for the Care and Use of Laboratory Animals published by the US National Institutes of Health and were approved by the Alberta Health Sciences Animal Policy and Welfare Committee. Adult (8 weeks old) male and female Sprague-Dawley rats ($n = 32$, 16 of each sex) were purchased from Charles River Canada. All animals were allowed access to food and water ad libitum throughout the experiment period and were maintained on a 12-h light/dark cycle.

2.3. Experimental design and abdominal aortic constriction surgery

Rats were kept in the animal facility for an acclimatization period of 1 week, after which both male and female rats were randomized into sham and abdominal aortic constriction (AAC) surgeries giving 4 groups: male sham ($n = 8$), male AAC ($n = 8$), female sham ($n = 8$), and female AAC ($n = 6$). Rats underwent baseline echocardiography before the surgeries.

For the surgeries, all rats were anesthetized with isoflurane (2% for induction and 1%–1.5% for maintenance). Preoperatively, meloxicam (Metacam) was injected subcutaneously at a dose of 2 mg/kg. The surgery was performed as described previously (Shoieb et al, 2022). The abdominal aorta was ligated using a double blunted needle sized 21 G for males and 23 G for females because of their different body weights, by 6/0 silk suture. Postoperatively, meloxicam was injected at a dose of 2 mg/kg every 24 hours for 72 hours.

Five weeks after the surgery, rats underwent echocardiography and then were euthanized using isoflurane anesthesia (3% induction and 1%–1.5% maintenance). Then, hearts were swiftly excised, washed with saline, and blotted with filter paper. After that, the left

ventricle was cut and homogenized using the Branson homogenizer (VWR Scientific).

2.4. Echocardiographic evaluation of cardiac function

All rats were anesthetized with isoflurane (2% for induction and 1%–1.5% for maintenance). Then, transthoracic m-mode echocardiography (Vevo 3100, VisualSonics) was performed using a small animal imaging ultrasound system to evaluate cardiac function and wall thickness. Images were taken and analyzed using VisualSonics Vevo LAB software. Systolic and wall measurements (left ventricular [LV] internal diameter, LV posterior wall thickness, and intra-ventricular septum [IVS]), LV mass, ejection fraction, fractional shortening, diastolic function, heart rate, and mitral tissue Doppler parameters were measured using m-mode measurements taken from parasternal long-axis and short-axis views at the mid-papillary level. LV dimensions were measured at systole and diastole. Pressure gradient (mm Hg) was measured from the abdominal aortic flow at the level of the constriction using the velocity–time integral measurement. Measurements were averaged from 3 to 6 cardiac cycles according to the American Society of Echocardiography (Byrd et al, 2015), digitally transferred online to a computer, and analyzed by an analyst blinded to the study groups.

2.5. RNA extraction and cDNA synthesis

TRIzol reagent (Invitrogen) was used to extract total RNA from the frozen tissue according to the manufacturer's instructions. RNA extraction, quantification, and cDNA synthesis were performed as described previously (Elshenawy and El-Kadi, 2015).

2.6. Real-time polymerase chain reaction

The resulting cDNA was subject to PCR amplification using 384-well optical reaction plates in the QuantStudio 5 (Applied

Biosystems). The 20- μ L reaction mix composition and thermocycling conditions were as described in previous reports (Shoieb et al, 2022). Rat primer sequences are listed in Table 1. Analysis of the real-time PCR data was performed using the relative gene expression ($\Delta\Delta$ CT) method (Livak and Schmittgen, 2001). In short, the fold change in the level of target genes between the groups, corrected for the level of the housekeeping gene, was determined using the following equation: Fold change = $2^{-\Delta(\Delta$ CT)}, where Δ CT = Ct(target gene) – Ct(housekeeping gene) and $\Delta(\Delta$ CT) = Δ CT(AAC) – mean Δ CT(sham).

2.7. Microsomal isolation

Microsomal fractions were prepared by differential centrifugation as described previously (Gerges and El-Kadi, 2023). The Lowry method was used to determine microsomal protein concentrations using bovine serum albumin as a standard (Lowry et al, 1951).

2.8. Western blot

We determined the protein expression of important CYP hydroxylases (CYP1A2, CYP1B1, CYP4A1, and CYP4F) and epoxigenases (CYP2J) in the heart microsomal fraction. Equal protein amounts (60 μ g) from the different groups were diluted with an equal amount of 2X Laemmli Sample Buffer, boiled for 5 minutes, and separated by 10% SDS-PAGE as described previously (Shoieb et al, 2022). Then, the blots were incubated with the primary antibody: mouse anti-CYP1A2, rabbit anti-rat CYP1B1, mouse anti-rat CYP4A1, rabbit antihuman CYP4F2, and rabbit anti-rat CYP2J overnight at 4 °C. Then, blots were incubated with a horseradish peroxidase–conjugated horse antimouse or goat anti-rabbit IgG secondary antibody for 45 minutes at room temperature. Bands were visualized using the ChemiDoc Imaging System (Bio-Rad Laboratories) using the enhanced chemiluminescence method.

Table 1
Rat primer sequences used for real-time PCR

Gene	Forward Primer	Reverse Primer
CYP1A1	CCAAACGAGTTCGGCCT	TGCCAAACCAAGAGAATGA
CYP1A2	CGCCAGAGCGGTTCTTA	TCCCAAGCCGAAGAGCATC
CYP1B1	GCTTTACTGTGCAAGGGAGACA	GGAAGGAGGATTCAAGTCAGGA
CYP2B1	AACCCCTTGATGACCGCAGTAAA	TGTGGTACTCCAATAGGGACAAGATC
CYP2B2	CCATCCCTTGATGATCGTACCA	AATTGGGGCAAGATCTGCAAA
CYP2C11	CACCAGCTATCAGTGGATTGG	GTCTGCCCTTTGCACAGGAA
CYP2C13	CTGGCAATCATGTGACTGA	GAAACTCCTTGCTGTCATGC
CYP2E1	AAAGCGTGTGTGTGTGGAGAA	AGAGACTTCAGGTTAAATGCTGCA
CYP2J3	CATTGAGCTCACAAAGTGGCTTT	CAATTCTAGGCTGTGATGTCG
CYP2J4	GCTCGACCTTCATTCCACA	GATCGTGGCTACCAGAGAGC
CYP2J10	TTGAACCTAGCAGAGGGGCTG	TCATACTCAAAGCGCTCCCC
CYP3A2	GCTCTTGATGCATGGTTAAAGATTG	ATCACAGACCTTGCCAACTCCTT
CYP4A1	TTGAGCTACTGCCAGATCCAC	CCCATTTTGGACTTCAGCACA
CYP4A2	CTCGCCATAGCCATGCTTATC	CCTTCAGCTCATTTCATGCAATT
CYP4A3	CTCGCCATAGCCATGCTTATC	CCTTCAGCTCATTTCATGCAATC
CYP4F1	CCCCAAGGCTTTTGTATG	GAGCGCAACGGCAGCT
CYP4F4	CAGGTCTGAAGCAGGTAAGTAAAGC	CCGTCAGGGTGGCACAGAGT
CYP4F5	AGGATGCCGTGGCTAACTG	GGCTCCAAGCAGCAGAAGA
CYP4F6	TCACTTGACCTTGATGAAGAACAAC	AAGAGAGGTGGATATCACGGAAG
ANP	GGAGCCTGCCAAGGTCAA	TATCTTCGGTACCGAAGGTGT
BNP	CAGAAGCTGCTGGAGCTGATAAG	TGTAGGGCCTTGGTCTTTG
ACTA1	AGAGTCAGAGCAGAGAACTAGA	CACGATGGATGGGAACACAGC
α -MHC	ACAGAGTGCTTCGTGCTGAT	CGAATTTCGGAGGGTCTGCTG
β -MHC	AGCTCCTAAGTAATCTGTTGCCAA	AAAGGATGAGCCTTTCTTTGCT
TNF- α	CAAGGTATCCATGACAACCTTG	GGGCCATCCACAGTCTTCTG
IL-1 β	GAAGTCAAGACCAAGTGG	TGAAGTCAACTATGTCCCG
IL-6	ATATGTTCTCAGGGAGATCTTGGAA	TGTCATCATCGCTGTTTCATACA
sEH	CACATCCAAGCCACCAAGCC	CAGGCCTCCATCTCCAG
GAPDH	CAAGGTATCCATGACAACCTTG	GGGCCATCCACAGTCTTCTG

ANP, atrial natriuretic peptide; BNP, brain natriuretic peptide; GAPDH, glyceraldehyde-3-phosphate dehydrogenase.

2.9. Microsomal incubation with AA

Isolated microsomes were incubated with AA as described previously (Gerges et al, 2023). The reaction started by adding 1-mM NADPH and incubating at 37 °C in a shaking water bath for 20 minutes. The reaction was then terminated by adding 600 μ L of ice-cold acetonitrile containing the internal standards (20-HETE-D6 for the HETEs assay and 11,12-EET-D11 for the EETs assay). HETE and EET metabolites were extracted with ethyl acetate and speed vacuum-dried (Savant SpeedVac SPD130DLX). Thereafter, samples were reconstituted with 100 μ L of acetonitrile and subjected to analysis.

2.10. Extraction of AA metabolites from the heart tissue

Two hundred milligrams of heart tissue were homogenized on ice with 2 mL methanol + 1% formic acid. The homogenates were centrifuged at 10,000g for 20 minutes at 4 °C. The supernatant was separated, and the internal standards 20-HETE-D6 and 11,12-EETD11 were added (1 μ L/mL). Metabolites were extracted from the supernatant by double extraction with 1 mL ethyl acetate and speed vacuum-dried (Savant SpeedVac SPD130DLX). Thereafter, samples were reconstituted with 100 μ L of acetonitrile and subjected to analysis.

2.11. Liquid chromatography-tandem mass spectrometry

The extracted AA metabolites (HETEs and EETs) were reconstituted in acetonitrile and then separated and quantified by a chiral liquid chromatography-tandem mass spectrometry assay that was optimized and validated for the separation of different HETE enantiomers (Isse et al, 2023a). Briefly, liquid chromatography was operated using a chiral stationary phase column (Reflect C-Amylose A column) and mobile phases consisting of an organic phase of acetonitrile, methanol, and isopropyl alcohol (88:6:6, v/v) + 0.1% acetic acid, and an aqueous phase of high-performance liquid chromatography water + 0.1% acetic acid. Metabolites were separated by gradient elution. Autosampler and column temperatures were set to 4 and 30 °C, respectively. The column was conditioned with 40% of the organic phase at a flow rate of 0.5 mL/min. The concentrations of metabolites were determined using calibration curves. The tandem mass spectrometry ionization mode was negative electrospray ionization, and each HETE had a specific product ion. The intrarun percent error and CV were both $\leq \pm 12\%$, and the interrun percent error and CV were $\leq \pm 13\%$ and $\leq 15\%$, respectively.

2.12. Statistical analysis

All data are represented as mean \pm SD. Heart weight:tibial length (HW:TL), echocardiographic data, and Western blot data were analyzed by unpaired Student's *t* test to compare each AAC group to the same-sex sham group. All other comparisons were conducted among different sex and surgery groups by two-way ANOVA, followed by Tukey's multiple comparison as a post hoc analysis. Correlation analyses were performed using Pearson or Spearman correlation, depending on data distribution. The normality of the data was assessed using the Shapiro-Wilk test. Differences were considered significant at $P < .05$. All statistical analyses and graphs plotting were performed using GraphPad Prism software, version 8.4.3. (GraphPad Software, Inc).

3. Results

3.1. Male rats develop a stronger hypertrophic response to AAC compared to female rats

Male and female rats were randomized to sham and AAC surgeries. Five weeks later, hypertrophy was assessed in vivo by ultrasound echocardiography and ex vivo by calculation of HW:TL ratio and measuring the mRNA expression of several fetal program genes that are reinduced in cardiomyocytes hypertrophy. Our results show that male rats develop more severe cardiac hypertrophy in response to AAC compared to female rats.

The HW:TL calculation and echocardiographic wall measurements demonstrate that male rats developed significant hypertrophy in response to AAC, as evidenced by the significant increase in the HW:TL, the LV posterior wall thickness systolic, intraventricular septum thickness systolic and diastolic (IVS;s and IVS;d), and the corrected LV mass by 13%, 13.5%, 18%, 10%, and 15% compared to male sham rats, respectively. On the other hand, female AAC rats demonstrated a significant increase only in IVS;s and IVS;d by 9% and 12%, respectively, compared to female sham rats, whereas they showed a nonsignificant increase in corrected LV mass and HW:TL. Only male rats demonstrated a significant decrease in the E'/A' by 26%, which indicates impaired relaxation of the ventricles and the beginning of diastolic dysfunction. In addition, only male rats developed a significant increase in the Tei index, which is also known as the myocardial performance index, by 13% due to AAC (Table 2). Figure 1 shows representative LV m-mode images from 2D-ultrasonic echocardiography taken 5 weeks post-AAC (A) and HW:TL ratio (B) in male and female rats.

In addition, the mRNA expression of the hypertrophic markers skeletal muscle alpha-actin (ACTA1) and the ratio of β - to α -myosin heavy chain (β/α -MHC) were significantly increased in the hearts of male AAC rats by 1.8- and 2-fold, respectively, compared to male sham rats, whereas they were not significantly increased in female rats. Moreover, mRNA levels of ACTA1, β/α -MHC, and brain natriuretic peptide were found to be significantly higher in the hearts of male AAC rats compared to female AAC rats by 2.1-, 2.2-, and 2.4-fold, respectively (Fig. 1C).

3.2. AAC-induced hypertrophy results in sexually dimorphic changes in the cardiac mRNA expression of CYP hydroxylases

AAC-induced cardiac hypertrophy was associated with a significant increase in the cardiac mRNA expression of CYP1A2 and CYP3A2 in male AAC rats by 12.5- and 9-fold, respectively, compared to male sham rats, but not in female rats. Moreover, the CYP1A2 mRNA level in male AAC hearts was significantly higher than in female AAC rats by 7.3-fold. In contrast, CYP2E1 mRNA level was found to be 2.8-fold higher in the hearts of female AAC rats compared to male AAC rats. In agreement with previous results (Gerges and El-Kadi, 2023), CYP1A1 heart level was found to be significantly higher in female rats than in male rats of the sham group. The cardiac mRNA expression of CYP hydroxylases in male and female rats is shown in Fig. 2.

3.3. AAC-induced hypertrophy results in sexually dimorphic changes in the cardiac mRNA expression of CYP ω -hydroxylases

CYP4A and CYP4F enzymes mainly catalyze the ω -hydroxylation of AA into 20-HETE. Interestingly, CYP4A1, 4A2, 4A3, and 4F4 mRNA levels were significantly elevated in the hearts of male AAC compared to male sham rats (1.8-, 33.8-, 25.2-, and 14.1-fold, respectively). Of those 4 enzymes, CYP4A2, 4A3, and 4F4 also showed significantly higher expression levels in male AAC

Table 2

Ultrasonic echocardiography data representing ventricular wall dimensions, cardiac function, and hemodynamic parameters

Echo parameter	Baseline				5 weeks post-AAC			
	Male sham	Male AAC	Female sham	Female AAC	Male sham	Male AAC	Female sham	Female AAC
Body weight (g)	328.7 ± 13.4	321.5 ± 9.5	207.8 ± 15.4	211.2 ± 18.6	487.3 ± 34.9	474.6 ± 29.6	253.6 ± 12.8	251.4 ± 18.7
Heart rate (bpm)	384.7 ± 25.9	361.5 ± 22.2	378.2 ± 28.2	374.5 ± 37.8	343.6 ± 34.8	332.5 ± 28.5	374 ± 34.3	367.9 ± 35.3
Wall measurements								
IVS;s (mm)	2.7 ± 0.2	2.7 ± 0.3	2.3 ± 0.2	2.2 ± 0.3	2.4 ± 0.1	2.8 ± 0.2*	2 ± 0.1	2.2 ± 0.1*
IVS;d (mm)	1.6 ± 0.1	1.7 ± 0.2	1.5 ± 0.1	1.5 ± 0.2	1.8 ± 0.1	2 ± 0.2*	1.4 ± 0.1	1.6 ± 0.2*
LVID;s (mm)	4.7 ± 0.6	4.6 ± 0.5	3.8 ± 0.5	3.9 ± 0.6	5 ± 0.6	5 ± 0.5	3.7 ± 0.3	3.9 ± 0.4
LVID;d (mm)	8 ± 0.5	8.1 ± 0.4	6.9 ± 0.3	6.9 ± 0.6	8.4 ± 0.6	8.6 ± 0.4	6.8 ± 0.2	7 ± 0.3
LVPW;s (mm)	2.6 ± 0.2	2.6 ± 0.1	2.3 ± 0.2	2.2 ± 0.2	2.5 ± 0.1	2.8 ± 0.2*	2.1 ± 0.1	2.2 ± 0.2
LVPW;d (mm)	1.6 ± 0.2	1.7 ± 0.2	1.5 ± 0.1	1.5 ± 0.2	1.7 ± 0.1	1.8 ± 0.1	1.4 ± 0.1	1.5 ± 0.2
Corrected LV mass (mg)	765.2 ± 89.5	805.2 ± 76.7	546.8 ± 33.7	557.7 ± 73.1	896.4 ± 90.9	1033 ± 71.9*	435.3 ± 23	571.4 ± 94.7 (<i>P</i> = .056)
Systolic function								
LVV;s (μL)	102.2 ± 27.5	96.9 ± 27.4	64.1 ± 20.4	69.2 ± 24.3	109.7 ± 16.1	118.4 ± 27.1	59.1 ± 10	67.1 ± 16
LVV;d (μL)	352.8 ± 52.6	357.1 ± 46.1	244.7 ± 22.7	252 ± 43.8	387.5 ± 58.3	403.6 ± 34.6	241.3 ± 22.1	255.4 ± 29.9
SV (μL)	256.6 ± 34.9	260.2 ± 51.3	179.2 ± 23.3	180.6 ± 16.1	276.6 ± 25.3	285.3 ± 26.6	175.9 ± 11.6	188.3 ± 17.6
CO (mL/min)	96 ± 12.9	93.8 ± 17.5	68.3 ± 7.5	68.8 ± 14	91 ± 12.1	94.9 ± 12.8	67.8 ± 6.3	69.5 ± 10.9
%EF	71.3 ± 5.4	72.5 ± 7.8	74.1 ± 6.4	73.2 ± 5.4	68.9 ± 5.9	70.8 ± 5.4	75.5 ± 3.8	74 ± 3.8
%FS	42.3 ± 4.5	43.7 ± 6.9	44.4 ± 5.7	43.5 ± 4.5	40.5 ± 4.9	42.1 ± 4.6	45.5 ± 3.5	44.2 ± 3.3
Diastolic function								
Mitral E/A	1.4 ± 0.3	1.7 ± 0.5	1.2 ± 0.1	1.3 ± 0.2	1.4 ± 0.3	1.3 ± 0.3	1.5 ± 0.3	1.3 ± 0.2
E'/A'	1 ± 0.3	1 ± 0.3	0.85 ± 0.3	0.8 ± 0.2	1 ± 0.2	0.75 ± 0.2*	1 ± 0.3	0.8 ± 0.1
E/E'	16.5 ± 2.2	16.9 ± 2.3	15.3 ± 3.2	17.25 ± 1.9	13 ± 2.8	15.9 ± 1.6*	15.3 ± 3.6	17.5 ± 1.4
S wave	51.9 ± 6	51.4 ± 6.1	46.3 ± 4.2	49 ± 3.1	53.6 ± 9.7	54.9 ± 10.3	46.3 ± 8	45.9 ± 3.5
Doppler imaging								
Tei index	0.5 ± 0.06	0.48 ± 0.1	0.5 ± 0.08	0.51 ± 0.09	0.49 ± 0.07	0.55 ± 0.06*	0.53 ± 0.1	0.51 ± 0.09
Abdominal aorta								
Peak pressure gradient (mm Hg)	0.58 ± 0.12	0.66 ± 0.22	0.7 ± 0.17	0.68 ± 0.15	0.77 ± 0.12	2.17 ± 0.54*	0.64 ± 0.09	2.21 ± 0.64*
Peak velocity (mm/s)	408 ± 79.8	380.1 ± 40.5	427.5 ± 50.7	435.4 ± 66.1	434.6 ± 28.4	757.5 ± 67.1*	407.9 ± 28.1	731.3 ± 111.9*

CO, cardiac output; EF, ejection fraction; E/A, wave velocity; E'/A', tissue Doppler wave; FS, fractional shortening; IVS;d, intraventricular septum diastolic; IVS;s, IVS systolic; LVID;d, left ventricular internal diameter diastolic; LVID;s, LVID systolic; LVPW;d, left ventricular posterior wall diastolic; LVPW;s, LVPW systolic; LVV, left ventricular volume; S, systolic tissue movement; SV, stroke volume; Tei index = (isovolumic relaxation time + isovolumic contraction time)/ejection time. Results are represented as mean ± SD, *n* = 6–8. Data were analyzed using unpaired Student's *t* test.

**P* < .05 compared to the same-sex sham post-AACs.

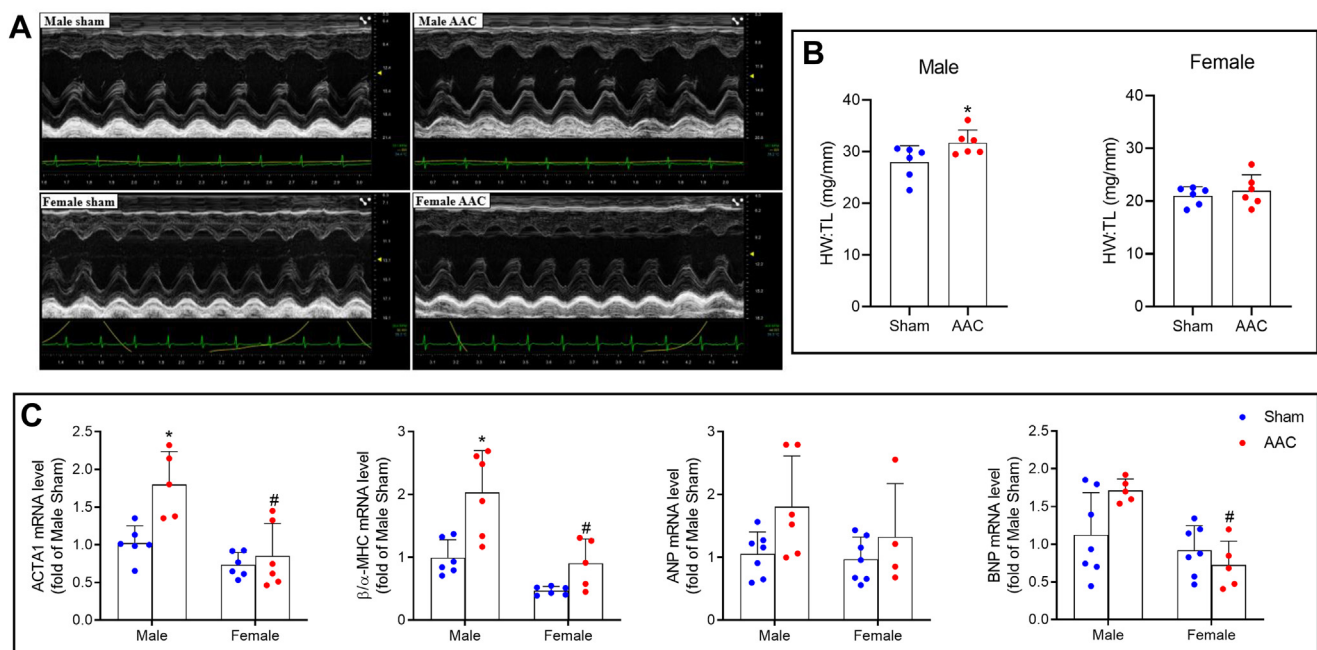


Fig. 1. Effect of abdominal aortic constriction (AAC)-induced hypertrophy on echocardiography, HW:TL ratio, and the mRNA expression of hypertrophic markers. Adult male and female Sprague–Dawley rats were subject to sham or AAC surgeries. Five weeks after the surgery, 2D ultrasonic echocardiography was conducted (A), the heart was isolated and HW:TL ratio was calculated (B), and the mRNA expression of the hypertrophic markers ACTA1, β-α-MHC, ANP, and BNP (C) was determined by real-time PCR. M-mode slices were taken in parasternal long axis mode. The results of all groups were normalized to the GAPDH housekeeping gene. Results are represented as mean ± SD, *n* = 4–7. HW:TL data were analyzed using unpaired Student's *t* test, **P* < .05 compared to same-sex sham, whereas hypertrophic markers data were analyzed using two-way ANOVA followed by Tukey's multiple comparison post hoc analysis, **P* < .05 compared to same-sex sham; #*P* < .05 compared to male rats of the same surgical group. ANP, atrial natriuretic peptide; BNP, brain natriuretic peptide; GAPDH, glyceraldehyde-3-phosphate dehydrogenase.

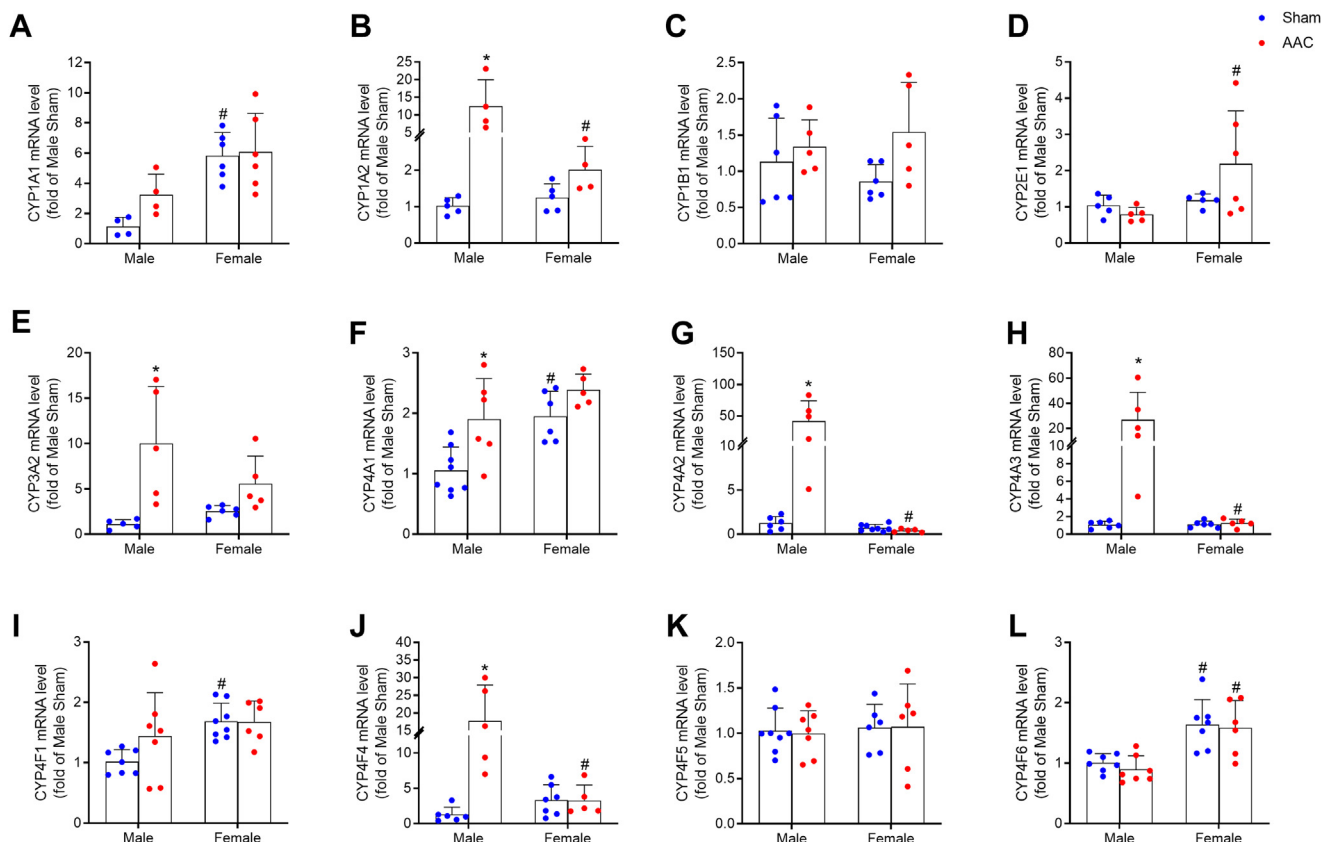


Fig. 2. Effect of abdominal aortic constriction (AAC)-induced hypertrophy on the mRNA expression of CYP hydroxylases and CYP ω -hydroxylases. Adult male and female Sprague–Dawley rats were subject to sham or AAC surgeries. Five weeks after the surgery, the heart was isolated, and the mRNA expression of CYP1A1 (A), CYP1A2 (B), CYP1B1 (C), CYP2E1 (D), CYP3A2 (E), CYP4A1 (F), CYP4A2 (G), CYP4A3 (H), CYP4F1 (I), CYP4F4 (J), CYP4F5 (K), and CYP4F6 (L) was determined by real-time PCR. The results of all groups were normalized to the GAPDH housekeeping gene. Results are represented as mean \pm SD, $n = 4-8$. Data were analyzed using two-way ANOVA followed by Tukey's multiple comparison post hoc analysis, * $P < .05$ compared to the same-sex sham; # $P < .05$ compared to male rats of the same surgical group. GAPDH, glyceraldehyde-3-phosphate dehydrogenase.

compared to female AAC rat hearts (102.2-, 21.6-, and 5.4-fold, respectively). On the other hand, none of the enzymes was significantly changed in the female rats due to AAC surgery. However, in agreement with previous results, CYP4A1, 4F1, and 4F6 were found to be significantly higher in female sham rats compared to male sham ones. The cardiac mRNA expression of CYP ω -hydroxylases in male and female rats is shown in Fig. 2.

3.4. AAC-induced hypertrophy results in sexually dimorphic changes in the cardiac mRNA expression of CYP epoxygenases

Interestingly, AAC-induced hypertrophy was accompanied by a significant 10.3-, 3.7-, 7.2-, and 1.8-fold increase in the mRNA expression of the epoxygenases CYP2B2, 2C11, 2C13, and 2J10, respectively, in the hearts of male but not female rats compared to their sham counterparts. In addition, CYP2B2, 2C13, and 2J10 levels were significantly higher in male rats compared to female AAC rats by 3.5-, 3.2-, and 1.9-fold, respectively. In contrast, CYP2B1 was significantly higher in female rat hearts compared to male AAC rat hearts, by 3-fold. CYP2J3 was found to be significantly higher in the hearts of female rats compared to male rats in both sham and AAC surgical groups. The cardiac mRNA expression of CYP epoxygenases in male and female rats is shown in Fig. 3.

3.5. AAC-induced hypertrophy results in sexually dimorphic changes in the cardiac protein expression of CYP enzymes

CYP1B1 plays a specifically important role in the production of midchain HETEs and the pathogenesis of cardiac hypertrophy.

Although the increase in CYP1B1 mRNA in both male and female AAC rats was not statistically significant compared to their respective sham groups, Western blot analysis of its protein expression showed a significant 2.4-fold increase in male AAC compared to male sham rats, while it was not significantly changed in female rats. In addition, cardiac CYP4A and CYP4F levels were significantly increased in male AAC rats by 1.5- and 1.3-fold, respectively, compared to male sham rats. In female rats, CYP4A shows a slight increase that was not statistically significant. Western blot analysis of CYP1A2 and CYP2J protein expression revealed no significant change due to AAC surgery in male or female rats. The cardiac protein expression of CYP enzymes in male and female rats is shown in Fig. 4.

3.6. AAC-induced hypertrophy results in sexually dimorphic changes in the cardiac microsomal formation of HETEs but has no effect on EETs

Interestingly, our results demonstrated sexual dimorphism in the effect of AAC on the HETE formation rate. The microsomal formation rate of both the R and S enantiomers of 9-, 11-, and 12-HETE were significantly increased in male AAC rats by 15% and 17.5%, 7% and 5%, and 15% and 14%, respectively, compared to male sham rats. The S enantiomer of 8-HETE and the R enantiomer of 15-HETE were significantly elevated in male AAC rats compared to sham rats by 15% and 12%, respectively. None of the midchain HETEs was significantly altered in female rats by AAC surgery.

HETEs that are formed by ω and $\omega-1$ hydroxylation of AA are termed subterminal (16-, 17-, 18-, and 19-HETE) and terminal

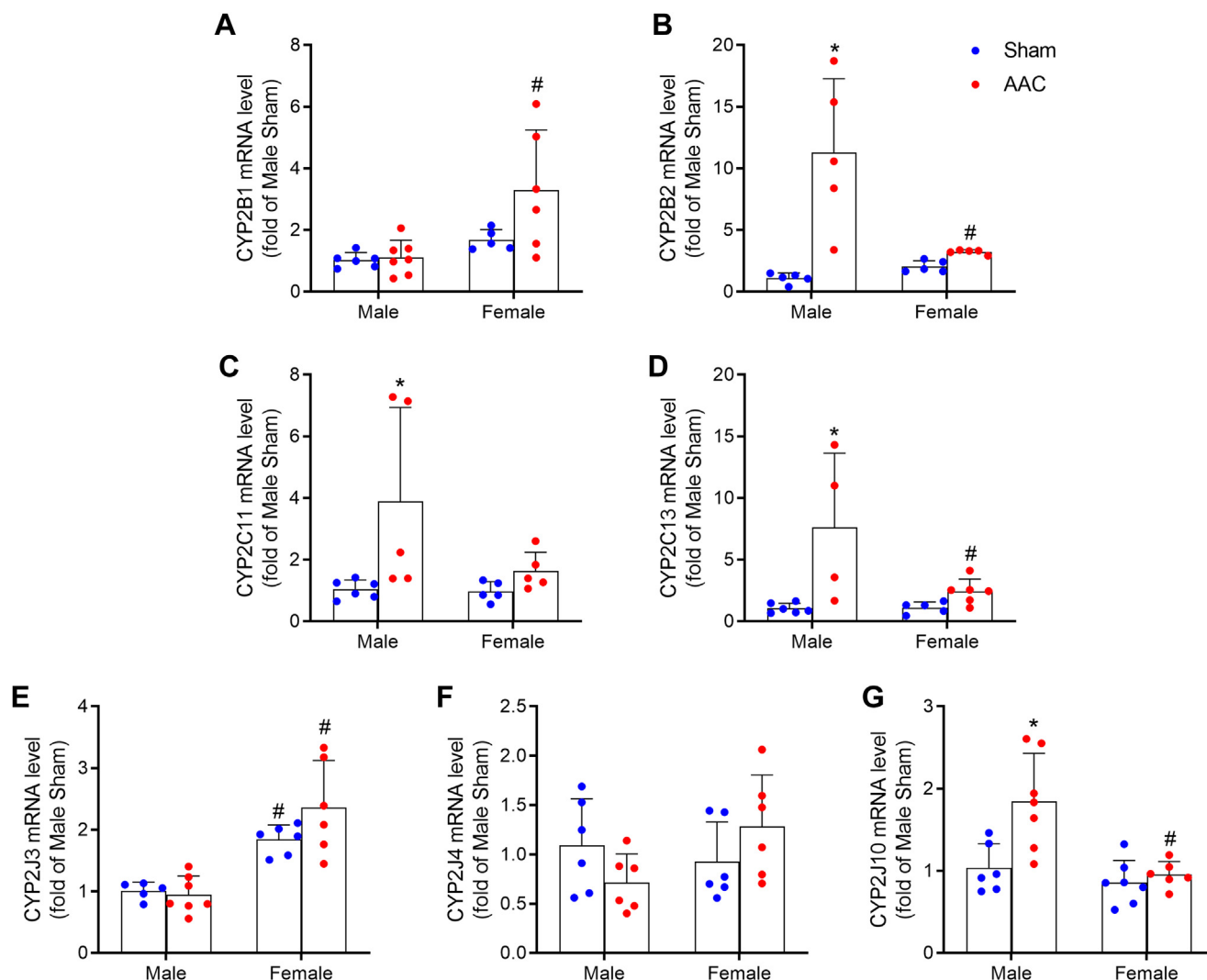


Fig. 3. Effect of abdominal aortic constriction (AAC)-induced hypertrophy on the mRNA expression of CYP epoxygenases. Adult male and female Sprague–Dawley rats were subject to sham or AAC surgeries. Five weeks after the surgery, the heart was isolated, and the mRNA expression of CYP2B1 (A), CYP2B2 (B), CYP2C11 (C), CYP2C13 (D), CYP2J3 (E), CYP2J4 (F), and CYP2J10 (G) was determined by real-time PCR. The results of all groups were normalized to the GAPDH housekeeping gene. Results are represented as mean \pm SD, $n = 5-7$. Data were analyzed using two-way ANOVA followed by Tukey's multiple comparison post hoc analysis, * $P < .05$ compared to the same-sex sham; # $P < .05$ compared to male rats of the same surgical group. GAPDH, glyceraldehyde-3-phosphate dehydrogenase.

(20-HETE) HETEs. We were able to detect 16-, 19-, and 20-HETE formation rates in the heart microsomes. We found no significant change in 16(R) or 16(S)-HETE formation rate in male or female rats due to AAC; however, we found a significant sex-specific difference as the formation of both R and S enantiomers of 16-HETE was significantly higher in male AAC rats than in female AAC rats by 129% and 162%, respectively. As for 20-HETE, there was a significant increase in its formation rate in AAC compared to sham groups, by 10% in males and 12% in females, but there was no sex-specific difference. The cardiac microsomal formation of all HETEs in male and female rats is shown in Fig. 5.

Microsomal formation rates of the different enantiomers of EETs were also investigated by liquid chromatography-tandem mass spectrometry. As shown in Fig. 6, we found no significant change in any of them attributed to either AAC-induced hypertrophy or sex.

3.7. AAC-induced hypertrophy results in sexually dimorphic changes in the cardiac tissue levels of HETEs

HETE metabolites were directly extracted from the heart tissue using a liquid–liquid extraction method and subject to analysis by

liquid chromatography-tandem mass spectrometry. We were able to detect both enantiomers of 5-, 11-, and 15-HETE and the R enantiomer of 12-HETE. As shown in Fig. 7, the basal heart level of 12(R)-HETE was significantly increased in male AAC rats by 90% compared to male sham rats. In addition, we found a significant sex-specific effect in 12(R)-HETE level because it was significantly 6.1- and 5.4-fold higher in male sham and AAC rats compared to female sham and AAC rats, respectively.

3.8. AAC-induced hypertrophy results in sexually dimorphic changes in the cardiac levels of IL-1 β

Multiple studies have demonstrated that pressure overload can stimulate an inflammatory response in the heart characterized by increased expression of inflammatory cytokines. In order to investigate whether AAC-induced cardiac hypertrophy was associated with inflammation in male and female rats, we investigated the mRNA expression of tumor necrosis factor- α (TNF- α), interleukin (IL)-1 β , and IL-6 in the hearts of male and female rats. We found a significant 1.9-fold increase in IL-1 β in male AAC compared to male sham rats, whereas TNF- α and IL-6 were not significantly affected,

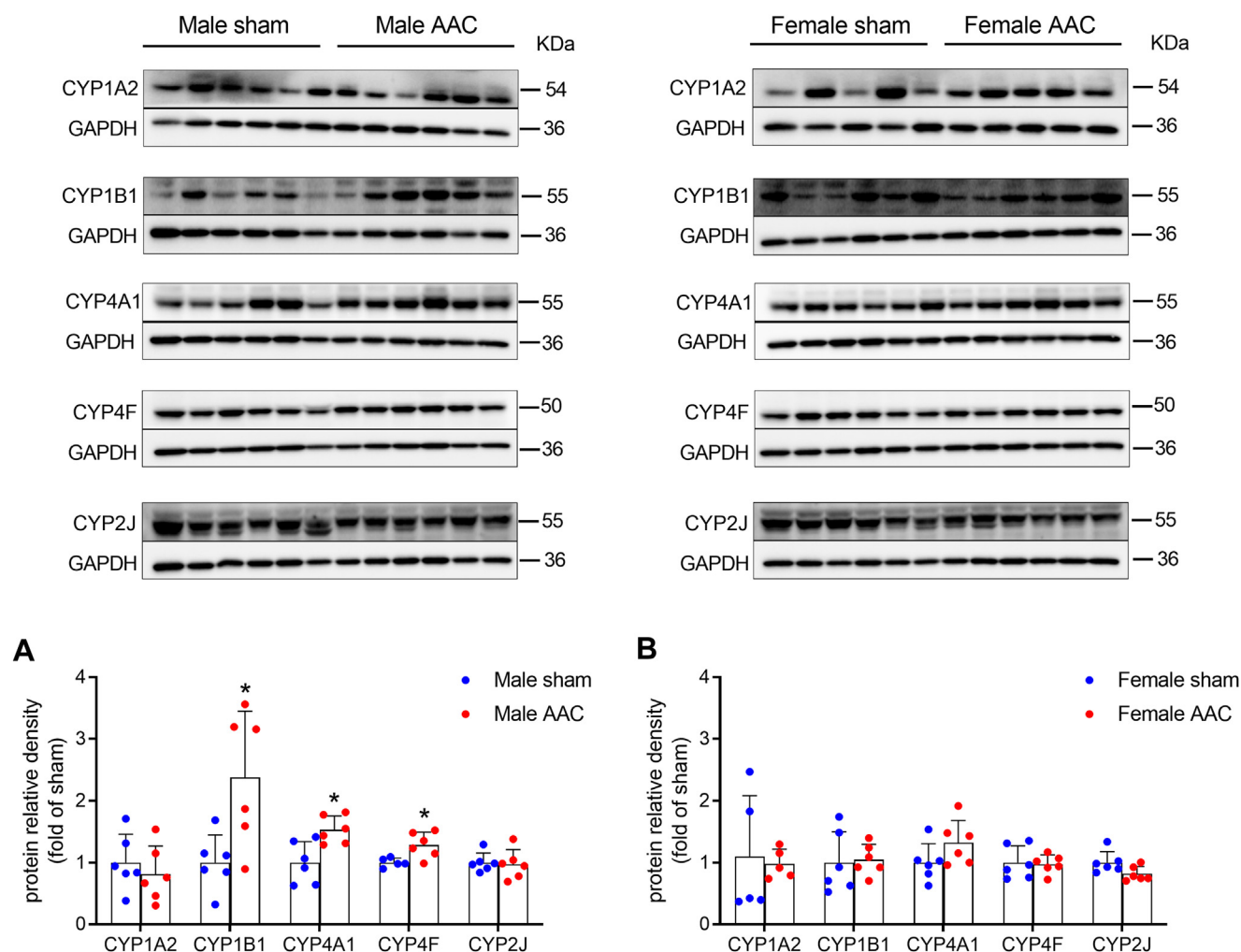


Fig. 4. Effect of abdominal aortic constriction (AAC)-induced hypertrophy on the protein expression of CYP enzymes. Adult male and female Sprague–Dawley rats were subject to sham or AAC surgeries. Five weeks after the surgery, heart microsomes were isolated, and the protein expression of CYP1A2, CYP1B1, CYP4A1, CYP4F, and CYP2J was determined in male (A) and female (B) rats by Western blot. The results of all groups were normalized to the GAPDH housekeeping protein. Results are represented as mean \pm SD, $n = 5–6$. Data were analyzed using unpaired Student's t test, * $P < .05$ compared to the same-sex sham. GAPDH, glyceraldehyde-3-phosphate dehydrogenase.

and none of them was significantly changed in female rats. Interestingly, we found that cardiac mRNA levels of IL-6 are significantly higher in female than in male rats by 2.6- and 2.7-fold for sham and AAC groups, respectively. The enzyme sEH breaks down EETs into less active metabolites. We found no significant change in sEH attributed either to AAC or to the rats' sex. The mRNA expression of TNF- α , IL-1 β , IL-6, and sEH in the heart is shown in Fig. 8.

3.9. Correlation between cardiac CYP enzyme expression and the degree of hypertrophy

CYP hydroxylases such as CYP1B1, CYP4A1, and CYP4F1 enzymes are known to be largely implicated in the pathogenesis of cardiac hypertrophy, and their inhibition or the antagonism of their products was found to ameliorate hypertrophy in several studies (El-Sherbeni and El-Kadi, 2014). Therefore, we conducted correlation analyses between the mRNA expression of CYP1B1, CYP4A1, and CYP4F1 and the mRNA expression of ACTA1, β/α -MHC, atrial natriuretic peptide, and brain natriuretic peptide. We found significant correlations between CYP4A1 and β/α -MHC in both male and female rats and between CYP4F1 and β/α -MHC only in male rats (Supplemental Fig. 1).

3.10. Correlation between cardiac CYP enzyme expression and the formation of HETEs

In order to further investigate the link between CYP hydroxylase protein expression and their metabolic activity expressed as HETE formation rate, we performed a correlation analysis between CYP1B1 protein expression and the formation of individual mid-chain HETEs in the hearts of male and female rats. Interestingly, we found a significant correlation between CYP1B1 protein level and the formation rates of both enantiomers of 5-, 8-, 12-, and 15-HETE, as well as the formation rates of 9(S)- and 11(S)-HETEs in male rats (Supplemental Fig. 2), while whereas in female rat hearts, no significant correlation was found (Supplemental Fig. 3). Moreover, we found a significant correlation between the protein levels of CYP4A1 and CYP4F enzymes in the hearts of male rats and the formation of 20-HETE, whereas in female rat hearts, the correlation was nonsignificant (Supplemental Fig. 4).

4. Discussion

Evidence from both experimental and clinical studies indicates significant sex-specific differences in the incidence and

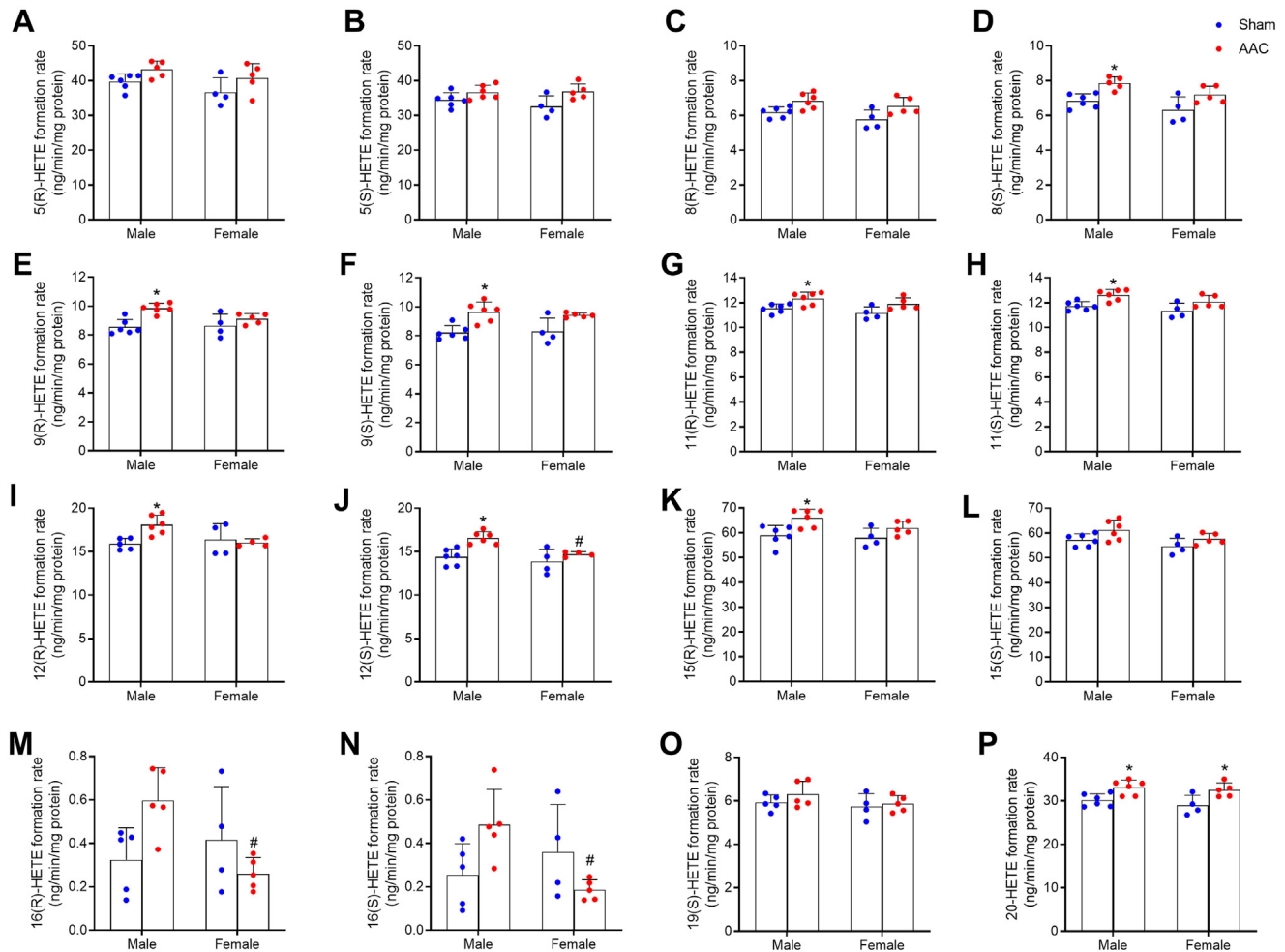


Fig. 5. Effect of abdominal aortic constriction (AAC)-induced hypertrophy on the formation of HETEs in the heart microsomes. Adult male and female Sprague–Dawley rats were subject to sham or AAC surgeries. Five weeks after the surgery, heart microsomes were isolated and incubated with arachidonic acid, and the formation of 5(R)-HETE (A), 5(S)-HETE (B), 8(R)-HETE (C), 8(S)-HETE (D), 9(R)-HETE (E), 9(S)-HETE (F), 11(R)-HETE (G), 11(S)-HETE (H), 12(R)-HETE (I), 12(S)-HETE (J), 15(R)-HETE (K), 15(S)-HETE (L), 16(R)-HETE (M), 16(S)-HETE (N), 19(S)-HETE (O), and 20-HETE (P) was determined by LC-MS/MS. Results are represented as mean \pm SD, $n = 4-6$. Data were analyzed using two-way ANOVA followed by Tukey's multiple comparison post hoc analysis, * $P < .05$ compared to the same-sex sham; # $P < .05$ compared to male rats of the same surgical group.

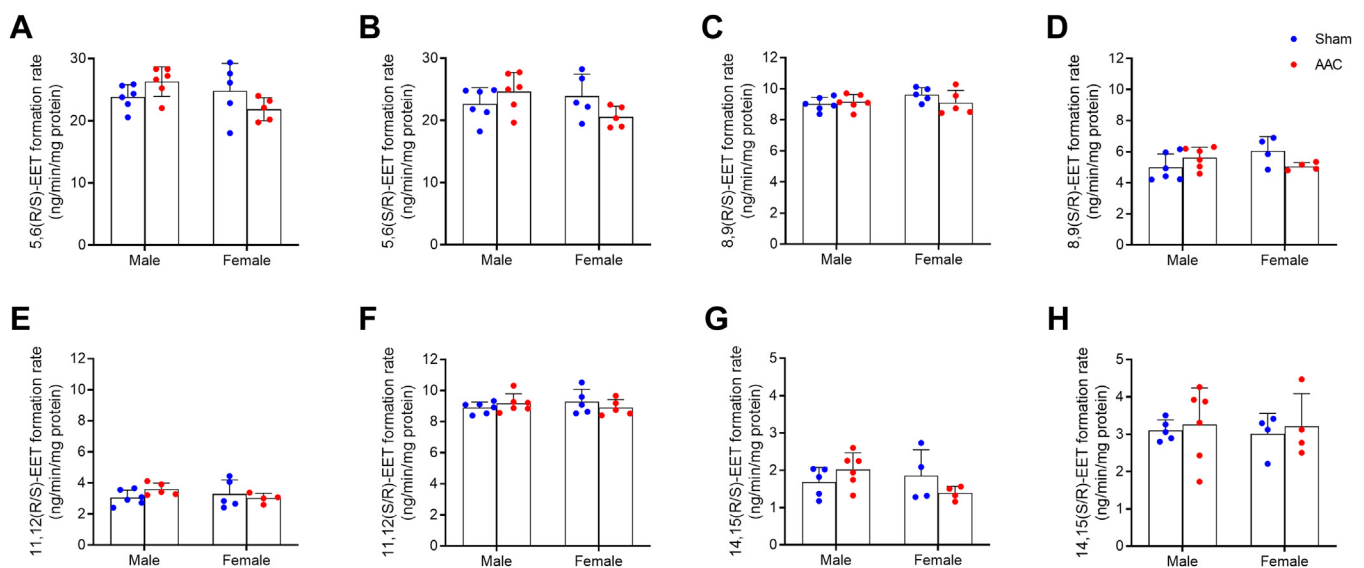


Fig. 6. Effect of abdominal aortic constriction (AAC)-induced hypertrophy on the formation of EETs in the heart microsomes. Adult male and female Sprague–Dawley rats were subject to sham or AAC surgeries. Five weeks after the surgery, heart microsomes were isolated and incubated with arachidonic acid, and the formation of 5,6(R/S)-EET (A), 5,6(S/R)-EET (B), 8,9(R/S)-EET (C), 8,9(S/R)-EET (D), 11,12(R/S)-EET (E), 11,12(S/R)-EET (F), 14,15(R/S)-EET (G), and 14,15(S/R)-EET (H) was determined by LC-MS/MS. Results are represented as mean \pm SD, $n = 4-6$. Data were analyzed using two-way ANOVA followed by Tukey's multiple comparison post hoc analysis. LC-MS/MS, liquid chromatography–tandem mass spectrometry.

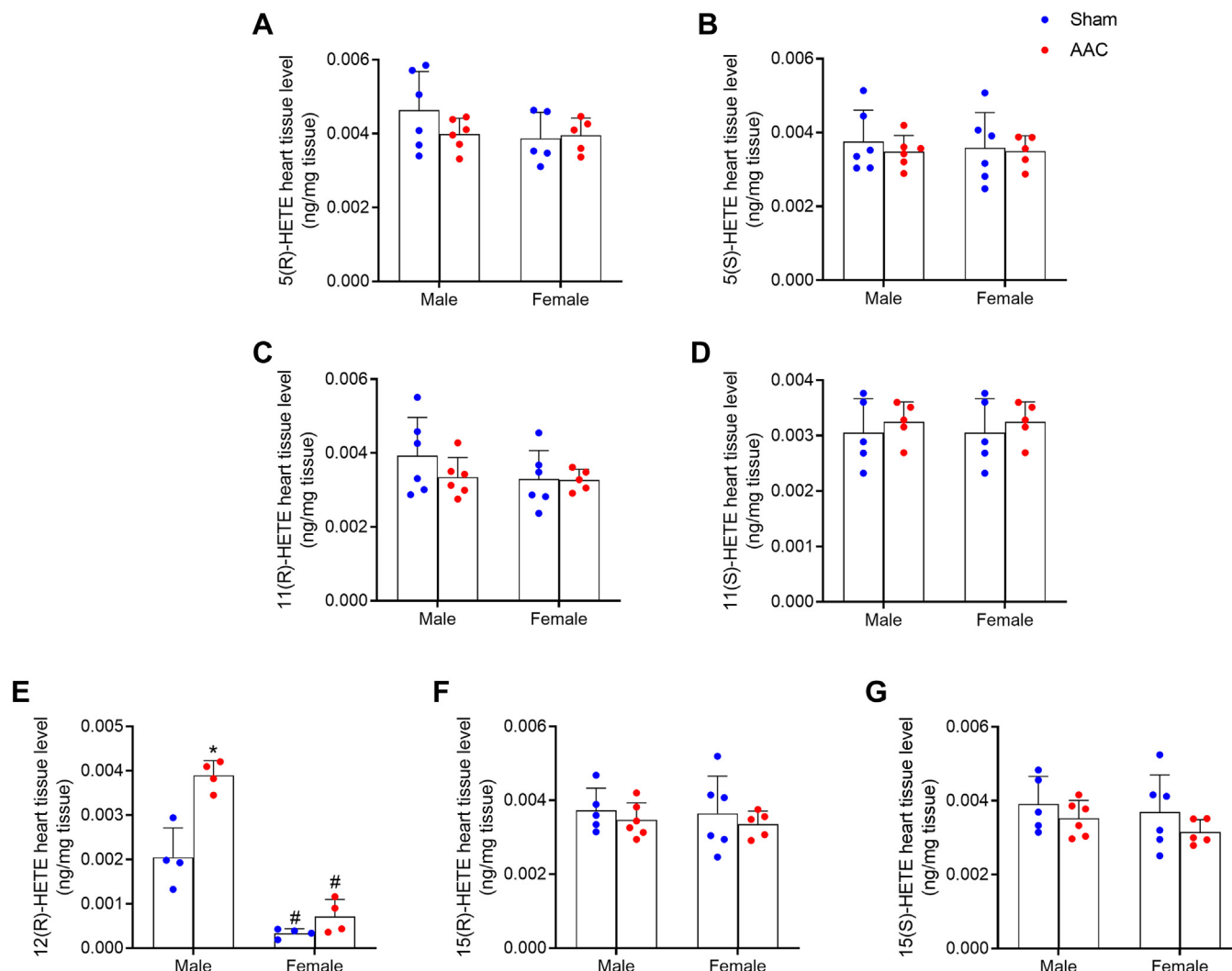


Fig. 7. Effect of abdominal aortic constriction (AAC)-induced hypertrophy on the basal heart levels of HETEs. Adult male and female Sprague–Dawley rats were subject to sham or AAC surgeries. Five weeks after the surgery, HETEs were extracted from the hearts by liquid–liquid extraction, and the levels of 5(R)-HETE (A), 5(S)-HETE (B), 11(R)-HETE (C), 11(S)-HETE (D), 12(R)-HETE (E), 15(R)-HETE (F), and 15(S)-HETE (G) were determined by LC-MS/MS. Results are represented as mean \pm SD, $n = 4$ –6. Data were analyzed using two-way ANOVA followed by Tukey's multiple comparison post hoc analysis, * $P < .05$ compared to the same-sex sham; # $P < .05$ compared to male rats of the same surgical group. LC-MS/MS, liquid chromatography–tandem mass spectrometry.

pathogenesis of different CVDs. Generally, several CVDs including cardiac hypertrophy and heart failure are less common and have a better prognosis in young women than in age-matched men (Regitz-Zagrosek and Kararigas, 2017); however, this advantage is lost after menopause (Rosano et al, 2007; El Khoudary et al, 2020). The exact mechanisms underlying these sex-specific differences are not yet fully elucidated, but they are largely attributed to the protective effects of estrogen on cardiovascular health (Regitz-Zagrosek and Kararigas, 2017).

In this study, cardiac hypertrophy was induced in male and female rats by AAC. In this model, the abdominal aorta is constricted between the right and the left renal arteries, leading to a state of pressure overload. This model leads to the gradual development of cardiac hypertrophy over several weeks, which mimics the clinical situation in humans with hypertensive heart disease or aortic stenosis. Compensated hypertrophy was successfully induced 5-weeks post-AAC specifically in male rats, as evidenced by the significant increase in the HW:TL ratio as well as several ventricular wall measurements and some hypertrophic markers, whereas female rats demonstrated strong protection.

Our results are in agreement with previous studies, which have also shown that females demonstrate stronger protection against pressure overload–induced hypertrophy than males (Ruppert et al, 2018; Kovács et al, 2024; Salehiyeh et al, 2024). The female sex protection can be attributed to higher estrogen levels and its effect through estrogen receptors such as estrogen receptor- β , which was found to mediate antihypertrophic effects (Skavdahl et al, 2005; Pedram et al, 2008; Fliegner et al, 2010). Clinically, women develop a more favorable form of hypertrophy that has a better prognosis compared to men (Regitz-Zagrosek and Kararigas, 2017). In addition, men more than women showed a persistent increase in LV diameter 1 week after aortic valve replacement surgery, whereas women demonstrated a reversal in their hypertrophy (Petrov et al, 2010).

AA metabolism by CYP enzymes produces eicosanoid metabolites including HETEs and EETs, which play important roles in the pathogenesis of cardiac hypertrophy (Elbekai and El-Kadi, 2006; Jenkins et al, 2009). For example, several HETEs promote the development of cardiac hypertrophy both directly through activating hypertrophic cellular signaling pathways and indirectly

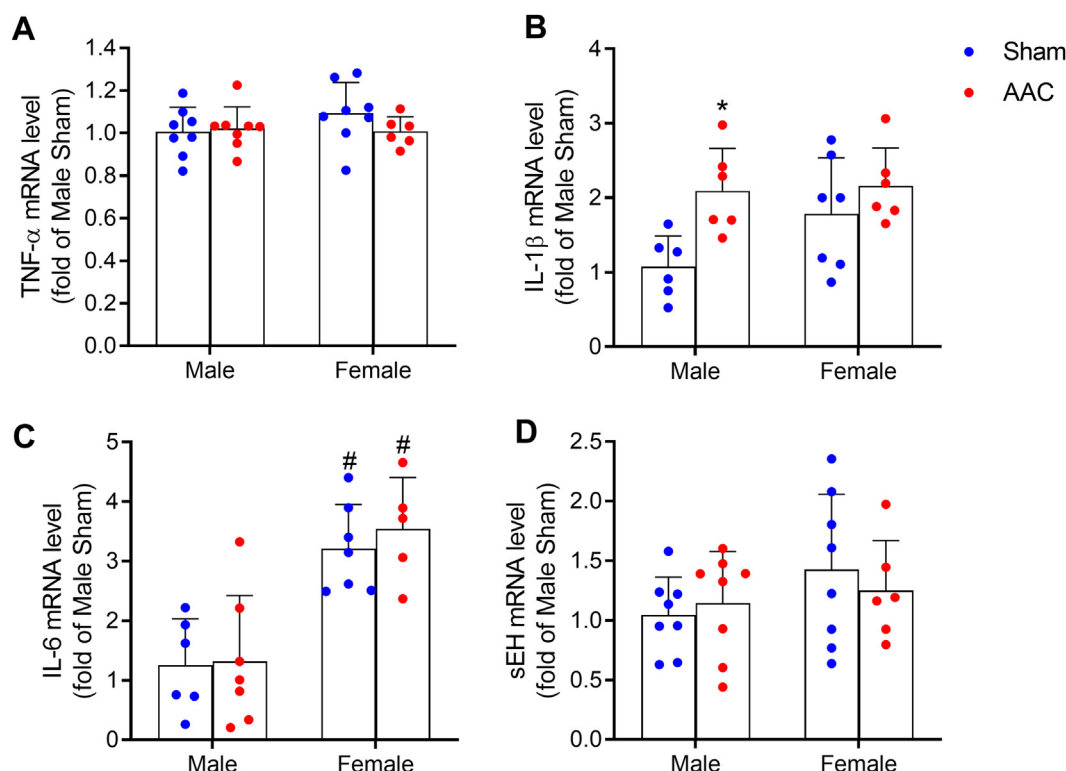


Fig. 8. Effect of abdominal aortic constriction (AAC)-induced hypertrophy on the mRNA expression of inflammatory cytokines and sEH. Adult male and female Sprague-Dawley rats were subject to sham or AAC surgeries. Five weeks after the surgery, the heart was isolated, and the mRNA expression of TNF- α (A), IL-1 β (B), IL-6 (C), and sEH (D) was determined by real-time PCR. The results of all groups were normalized to the GAPDH housekeeping gene. Results are represented as mean \pm SD, $n = 6-8$. Data were analyzed using two-way ANOVA followed by Tukey's multiple comparison post hoc analysis, * $P < .05$ compared to the same-sex sham; # $P < .05$ compared to male rats of the same surgical group. GAPDH, glyceraldehyde-3-phosphate dehydrogenase.

through promotion of underlying diseases such as hypertension and vascular diseases (Maayah and El-Kadi, 2016b). Several studies from our laboratory have found significant changes in CYP-mediated AA metabolism in different models of cardiac hypertrophy (Zordoky et al, 2008; Zordoky and El-Kadi, 2008; El-Sherbeni and El-Kadi, 2014; Maayah et al, 2017). Importantly, sex differences in CVDs can be attributed to differences between males and females in underlying molecular mechanisms such as enzyme expression and activity as well as metabolite levels (Gerges and El-Kadi, 2022). Notably, our previous studies have shown significant differences between male and female rats in the cardiac levels of CYP enzymes and HETEs (Gerges et al, 2023; Gerges and El-Kadi, 2023). Thus, in this study, we aimed to investigate sex-dependent changes in the cardiac levels of CYP enzymes and their AA metabolites in response to AAC-induced cardiac hypertrophy.

We found that AAC-induced hypertrophy was associated with a significant increase in the expression of the CYP hydroxylases CYP1B1, CYP1A2, and CYP3A2 only in male rats. CYP hydroxylases play an important role in the production of different midchain HETEs (Westphal et al, 2015; El-Sherbeni and El-Kadi, 2017). Interestingly, we found a significant correlation between the cardiac protein expression of CYP1B1 and the formation of several midchain HETEs in the hearts of male rats. CYP1B1 and its associated midchain HETEs are significantly elevated in pressure overload, isoproterenol, and angiotensin models of cardiac hypertrophy (Zordoky et al, 2008; El-Sherbeni and El-Kadi, 2014; Maayah et al, 2017). Moreover, CYP1B1 inhibition was associated with a reduction in midchain HETEs levels and amelioration of hypertrophy in several in vitro and in vivo models, indicating their crucial role in the development and progression of cardiac

hypertrophy (Elkhatali et al, 2017; Maayah et al, 2017, 2018; Shoieb and El-Kadi, 2018, 2020; Shoieb et al, 2022). Interestingly, multiple midchain HETEs were found to directly induce cellular hypertrophy in human fetal ventricular cardiomyocytes such as 5-, 8-, 11-, 12-, and 15-HETEs (Maayah et al, 2015; Maayah and El-Kadi, 2016a; Hidayat et al, 2023). In the current study, the increase in CYP hydroxylases in male AAC rats was associated with a significant increase in several midchain HETEs only in male rats. In addition, we found 12(R)-HETE level in the heart to be significantly higher in male rats than in female rats. Moreover, its level was significantly increased in males due to AAC hypertrophy. Interestingly, 12-HETE levels were found to be significantly elevated in cardiac hypertrophy and heart failure models, and it is known to activate hypertrophic signaling pathways and drive heart failure development (El-Sherbeni and El-Kadi, 2014; Matsumura et al, 2018; Berkowicz et al, 2019; Pascale et al, 2021).

AAC-induced hypertrophy was also associated with a significant increase in the expression of CYP4A and CYP4F enzymes in the hearts of male rats only but not female rats. Previous hypertrophy models have given conflicting results regarding CYP4A and 4F levels (Zordoky et al, 2008; El-Sherbeni and El-Kadi, 2014). CYP4A and CYP4F enzymes catalyze the ω -hydroxylation of AA-producing 20-HETE (Kroetz and Zeldin, 2002), which is known to exhibit cardiotoxic effects. Notably, 20-HETE promotes hypertension and cardiac injury by enhancing vasoconstriction, endothelial cell dysfunction, and inflammation. Moreover, 20-HETE is largely implicated in the pathophysiology of cardiac hypertrophy (Waldman et al, 2016; Rocić and Schwartzman, 2018). The 20-HETE levels were significantly elevated in multiple models of cardiac hypertrophy (El-Sherbeni and El-Kadi, 2014; Elkhatali et al, 2015),

and inhibition of its synthesis offered partial protection against the development of benzo(a)pyrene-induced cardiac hypertrophy (Aboutabl et al, 2009). In addition, a 20-HETE antagonist successfully attenuated cardiac hypertrophy in angiotensin-dependent hypertension (Sedláková et al, 2018). We found a significant increase in 20-HETE microsomal formation rate in both male and female rats. Interestingly, the formation of 20-HETE in male rats was found to be significantly correlated with the protein levels of both CYP4A1 and CYP4F enzymes. Moreover, the mRNA expression of these enzymes was significantly correlated to the degree of hypertrophy expressed as β/α -MHC ratio, which highlights their involvement in the development of hypertrophy and the potential implication of 20-HETE in this process. The increase in 20-HETE in female heart microsomes can be attributed to increased CYP4A or 4F enzyme activity, regardless of the expression level.

Similar to the increase in CYP hydroxylases, we found a significant increase in the mRNA level of several CYP epoxygenases such as CYP2B2, 2C11, 2C13, and 2J10 only in male rats, whereas none of them significantly changed in female rats due to AAC. This is in agreement with a previous study on DAC-induced hypertrophy (El-Sherbeni and El-Kadi, 2014). This result can be considered paradoxical because CYP epoxygenases mainly catalyze the production of EETs, which exhibit cardioprotective effects through their anti-inflammatory, antiapoptotic, antifibrotic, and antihypertrophic effects (Tse et al, 2013; Yang et al, 2015; Zhang et al, 2022). However, the classification of CYP enzymes into epoxygenases and hydroxylases is not a strict classification because each enzyme can produce eicosanoids from both classes of metabolites. In addition, the elevation in epoxygenases in males could have emerged as a compensatory mechanism to counteract the hypertrophic injury by attempting to increase EET production.

Despite the changes we found in CYP epoxygenases in AAC males, we found no significant change in EET microsomal formation in either sex. EETs are rapidly metabolized by sEH, which could potentially explain why we could not see any changes in their levels. Administration of a sEH inhibitor significantly ameliorated angiotensin-induced hypertrophy as shown by echocardiography, smaller cardiomyocyte size, and lower expression of hypertrophic markers (Ai et al, 2009). Previous studies have shown conflicting results regarding the changes in the heart levels of sEH in response to hypertrophy (Zordoky et al, 2008; Ai et al, 2009; El-Sherbeni and El-Kadi, 2014), and our study showed no significant change. These discrepancies could be attributed to the different models used (El-Sherbeni and El-Kadi, 2014). Generally, the AAC model can be considered less aggressive than other hypertrophy models, including other pressure overload models such as transverse aortic constriction and DAC, in which the constriction is closer to the heart, leading to a greater degree of pressure overload.

It is well known that the biological properties of different enantiomers of the same chiral drug or molecule can be different (Campo et al, 2009). Notably, enantiospecific properties and effects of different HETEs were demonstrated in several previous studies from our laboratory (Shoieb and El-Kadi, 2018; Hidayat et al, 2023; Isse et al, 2023b; Helal et al, 2024; Hidayat et al, 2024). Thus, we consider it important to investigate the effect of AAC on the formation of both enantiomers of each AA metabolite, and we did find some enantiospecific changes. More studies are needed to further investigate the different receptors and downstream signaling mechanisms of different enantiomers.

Inflammation is a hallmark of pathological cardiac hypertrophy and heart failure (Liu et al, 2021; ElKhatib et al, 2023). Several studies have shown elevated myocardial and circulating levels of TNF- α , IL-6, and IL-1 β in heart failure patients (Amin et al, 2020). Furthermore, inflammatory cytokines can exert prohypertrophic effects by activating signaling pathways that could drive

hypertrophy and heart failure (ElKhatib et al, 2024). Previous studies found an increase in heart or serum inflammatory cytokine levels in AAC-induced hypertrophy (Li et al, 2014; Tang et al, 2016; Meng et al, 2020). However, we only found a significant increase in IL-1 β in male AAC rats. Notably, testosterone was found to increase IL-1 β expression on macrophages and mast cells in male mice with myocarditis, together with other genes associated with cardiac remodeling (Frisancho-Kiss et al, 2007; Diaconu et al, 2021). Although we found no sex-specific difference in the cardiac mRNA levels of TNF- α , male rats may be more sensitive to its effects because of potentially higher levels of its receptors. A previous study found higher mRNA expression of TNF receptors (both type I and type II) in the hearts of male compared to female mice and concluded that its sex-specific differential expression may contribute to sex differences in heart failure severity (Kadokami et al, 2000). Despite the higher levels of IL-6 in the hearts of female rats, the presence of higher estrogen levels and its signaling through receptors such as estrogen receptor- β may overcome the inflammatory effects of IL-6 and may even bias its signaling toward protective anti-inflammatory signaling (Kararigas et al, 2011; Kessler et al, 2019).

5. Conclusion

In conclusion, in this study, pressure overload induced by AAC surgery resulted in cardiac hypertrophy that was significantly different between male and female rats. Male rats developed a much stronger hypertrophic response, whereas female rats exhibited significant protection against AAC-induced hypertrophy. Cardiac hypertrophy also resulted in sexually dimorphic changes in the cardiac CYP-mediated AA metabolism. We found a significant increase in several CYP hydroxylases, CYP epoxygenases, and different HETEs only in the hearts of male rats. Understanding some of the molecular mechanisms that underlie sexual dimorphism in cardiac hypertrophy and heart failure is a great step toward the development of personalized and more effective diagnostic and treatment strategies for both men and women.

There are several limitations to our work that should be acknowledged. First, although we investigated sex-specific differences between male and female rats, we did not investigate the effects of sex hormones on cardiac hypertrophy through gonadectomy and infusion. Another limitation of the current study is the lack of histological analysis to evaluate cardiac fibrosis, particularly using picrosirius red staining.

Abbreviations

AA, arachidonic acid; AAC, abdominal aortic constriction; ACTA1, skeletal muscle alpha-actin; CVDs, cardiovascular diseases; CYP, Cytochrome P450; EETs, epoxyeicosatrienoic acids; HETEs, hydroxyeicosatetraenoic acids; HW:TL, heart weight:tibial length; IL, interleukin; IVS, interventricular septum; LV, left ventricular; PCR, polymerase chain reaction; sEH, soluble epoxide hydrolase; TNF, tumor necrosis factor; β/α -MHC, β - to α -myosin heavy chain.

Financial support

This work was supported by a grant from the Canadian Institutes of Health Research (CIHR 168846) to A.O.S.E. S.H.G. is the recipient of Alberta Innovates Graduate Student Scholarship.

Conflict of interest

The authors declare no conflicts of interest.

Data availability

The authors declare that all the data supporting the findings of this study are contained within the paper and its Supplemental Data and/or available on request from the corresponding author.

Authorship contributions

Participated in research design: Gerges, El-Kadi.

Conducted experiments: Gerges, Helal, Silver.

Performed data analysis: Gerges, Silver.

Wrote or contributed to the writing of the manuscript: Gerges, Helal, Dyck, El-Kadi.

Supplemental material

This article has supplemental material available at dmd.aspetjournals.org.

References

- Aboutabl ME, Zordoky BN, and El-Kadi AO (2009) 3-methylcholanthrene and benzo(a)pyrene modulate cardiac cytochrome P450 gene expression and arachidonic acid metabolism in male Sprague Dawley rats. *Br J Pharmacol* **158**: 1808–1819.
- Ai D, Pang W, Li N, Xu M, Jones PD, Yang J, Zhang Y, Chiamvimonvat N, Shyy JY, Hammock BD, et al (2009) Soluble epoxide hydrolase plays an essential role in angiotensin II-induced cardiac hypertrophy. *Proc Natl Acad Sci U S A* **106**: 564–569.
- Althurwi HN, Maayah ZH, Elshenawy OH, and El-Kadi AO (2015) Early changes in cytochrome P450s and their associated arachidonic acid metabolites play a crucial role in the initiation of cardiac hypertrophy induced by isoproterenol. *Drug Metab Dispos* **43**:1254–1266.
- Amin MN, Siddiqui SA, Ibrahim M, Hakim ML, Ahammed MS, Kabir A, and Sultana F (2020) Inflammatory cytokines in the pathogenesis of cardiovascular disease and cancer. *SAGE Open Med* **8**:2050312120965752.
- Berkowicz P, Kij A, Walczak M, and Chlopicki S (2019) Eicosanoid profiling in effluent of isolated perfused heart of Tgα⁴⁴ mice with advanced heart failure. *J Physiol Pharmacol* **70**:135–142.
- Byrd BF 3rd, Abraham TP, Buxton DB, Coletta AV, Cooper JH, Douglas PS, Gillam LD, Goldstein SA, Graf TR, Horton KD, et al (2015) A summary of the American Society of Echocardiography Foundation value-based healthcare: summit 2014: the role of cardiovascular ultrasound in the new paradigm. *J Am Soc Echocardiogr* **28**:755–769.
- Campo VL, Bernardes LS, and Carvalho I (2009) Stereoselectivity in drug metabolism: molecular mechanisms and analytical methods. *Curr Drug Metab* **10**: 188–205.
- Chaudhary KR, Batchu SN, and Seubert JM (2009) Cytochrome P450 enzymes and the heart. *IUBMB Life* **61**:954–960.
- Diaconu R, Donoiu I, Mirea O, and Bălșeanu TA (2021) Testosterone, cardiomyopathies, and heart failure: a narrative review. *Asian J Androl* **23**:348–356.
- dos Santos RL, da Silva FB, RF Ribeiro Jr, and Stefanon I (2014) Sex hormones in the cardiovascular system. *Horm Mol Biol Clin Invest* **18**:89–103.
- El Khoudary SR, Aggarwal B, Beckie TM, Hodis HN, Johnson AE, Langer RD, Limacher MC, Manson JE, Stefanick ML, and Allison MA (2020) Menopause transition and cardiovascular disease risk: implications for timing of early prevention: a scientific statement from the American Heart Association. *Circulation* **142**:e506–e532.
- Elbekai RH and El-Kadi AO (2006) Cytochrome P450 enzymes: central players in cardiovascular health and disease. *Pharmacol Ther* **112**:564–587.
- Elkhatali S, El-Sherbeni AA, Elshenawy OH, Abdelhamid G, and El-Kadi AO (2015) 19-Hydroxyeicosatetraenoic acid and isoniazid protect against angiotensin II-induced cardiac hypertrophy. *Toxicol Appl Pharmacol* **289**:550–559.
- Elkhatali S, Maayah ZH, El-Sherbeni AA, Elshenawy OH, Abdelhamid G, Shoiab SM, and El-Kadi AOS (2017) Inhibition of mid-chain HETEs protects against angiotensin II-induced cardiac hypertrophy. *J Cardiovasc Pharmacol* **70**:16–24.
- ElKhatib MAW, Gerges SH, Isse FA, and El-Kadi AOS (2024) Cytochrome P450 1B1 is critical in the development of TNF-α, IL-6, and LPS-induced cellular hypertrophy. *Can J Physiol Pharmacol* **102**:408–421.
- ElKhatib MAW, Isse FA, and El-Kadi AOS (2023) Effect of inflammation on cytochrome P450-mediated arachidonic acid metabolism and the consequences on cardiac hypertrophy. *Drug Metab Rev* **55**:50–74.
- Elshenawy OH and El-Kadi AO (2015) Modulation of aryl hydrocarbon receptor regulated genes by acute administration of trimethylarsine oxide in the lung, kidney and heart of C57BL/6 mice. *Xenobiotica* **45**:930–943.
- El-Sherbeni AA and El-Kadi AO (2014) Alterations in cytochrome P450-derived arachidonic acid metabolism during pressure overload-induced cardiac hypertrophy. *Biochem Pharmacol* **87**:456–466.
- El-Sherbeni AA and El-Kadi AO (2017) Microsomal cytochrome P450 as a target for drug discovery and repurposing. *Drug Metab Rev* **49**:1–17.
- Fliegner D, Schubert C, Penkalla A, Witt H, Kararigas G, Dworatzek E, Staub E, Martus P, Ruiz Noppinger P, Kintscher U, et al (2010) Female sex and estrogen receptor-beta attenuate cardiac remodeling and apoptosis in pressure overload. *Am J Physiol Regul Integr Comp Physiol* **298**:R1597–R1606.
- Frisancho-Kiss S, Davis SE, Nyland JF, Frisancho JA, Cihakova D, Barrett MA, Rose NR, and Fairweather D (2007) Cutting edge: cross-regulation by TLR4 and T cell Ig mucin-3 determines sex differences in inflammatory heart disease. *J Immunol* **178**:6710–6714.
- Gerges SH and El-Kadi AOS (2022) Sex differences in eicosanoid formation and metabolism: a possible mediator of sex discrepancies in cardiovascular diseases. *Pharmacol Ther* **234**:108046.
- Gerges SH and El-Kadi AOS (2023) Sexual dimorphism in the expression of cytochrome P450 enzymes in rat heart, liver, kidney, lung, brain, and small intestine. *Drug Metab Dispos* **51**:81–94.
- Gerges SH, Alammari AH, El-Ghiaty MA, Isse FA, and El-Kadi AOS (2023) Sex- and enantiospecific differences in the formation rate of hydroxyeicosatetraenoic acids in rat organs. *Can J Physiol Pharmacol* **101**:425–436.
- Helal SA, El-Sherbeni AA, and El-Kadi AOS (2024) 11-Hydroxyeicosatetraenoic acid induces cellular hypertrophy in an enantioselective manner. *Front Pharmacol* **15**:1438567.
- Hidayat R, El-Ghiaty MA, Shoiab SM, Alqahtani MA, and El-Kadi AOS (2023) The effects of 16-HETE enantiomers on hypertrophic markers in human fetal ventricular cardiomyocytes, RL-14 cells. *Eur J Drug Metab Pharmacokinet* **48**: 709–722.
- Hidayat R, Shoiab SM, Mosa FES, Barakat K, Brocks DR, Isse FA, Gerges SH, and El-Kadi AOS (2024) 16R-HETE and 16S-HETE alter human cytochrome P450 1B1 enzyme activity probably through an allosteric mechanism. *Mol Cell Biochem* **479**:1379–1390.
- Isse FA, Alammari AH, El-Sherbeni AA, Brocks DR, and El-Kadi AOS (2023a) The enantioselective separation and quantitation of the hydroxy-metabolites of arachidonic acid by liquid chromatography–tandem mass spectrometry. *Prostaglandins Other Lipid Mediat* **165**:106701.
- Isse FA, Alammari AH, El-Sherbeni AA, and El-Kadi AOS (2023b) 17-(R/S)-hydroxyeicosatetraenoic acid (HETE) induces cardiac hypertrophy through the CYP1B1 in enantioselective manners. *Prostaglandins Other Lipid Mediat* **168**:106749.
- Jenkins CM, Cedars A, and Gross RW (2009) Eicosanoid signalling pathways in the heart. *Cardiovasc Res* **82**:240–249.
- Kadokami T, McTiernan CF, Kubota T, Frye CS, and Feldman AM (2000) Sex-related survival differences in murine cardiomyopathy are associated with differences in TNF-receptor expression. *J Clin Invest* **106**:589–597.
- Kararigas G, Fliegner D, Gustafsson J, and Regitz-Zagrosek V (2011) Role of the estrogen/estrogen-receptor-beta axis in the genomic response to pressure overload-induced hypertrophy. *Physiol Genomics* **43**:438–446.
- Kessler EL, Rivaud MR, Vos MA, and van Veen TAB (2019) Sex-specific influence on cardiac structural remodeling and therapy in cardiovascular disease. *Biol Sex Differ* **10**:7.
- Kovács A, Zhazykbayeva S, Herwig M, Fülöp G, Csipő T, Oláh N, Hassoun R, Budde H, Osman H, Kaçmaz M, et al (2024) Sex-specific cardiovascular remodeling leads to a divergent sex-dependent development of heart failure in aged hypertensive rats. *GeroScience* **46**:4543–4561.
- Kroetz DL and Zeldin DC (2002) Cytochrome P450 pathways of arachidonic acid metabolism. *Curr Opin Lipidol* **13**:273–283.
- Lai J and Chen C (2021) The role of epoxyeicosatrienoic acids in cardiac remodeling. *Front Physiol* **12**:642470.
- Li J, Li L, Chu H, Sun X, and Ge Z (2014) Oral sophocarpine protects rat heart against pressure overload-induced cardiac fibrosis. *Pharm Biol* **52**:1045–1051.
- Liu X, Shi GP, and Guo J (2021) Innate immune cells in pressure overload-induced cardiac hypertrophy and remodeling. *Front Cell Dev Biol* **9**:659666.
- Livak KJ and Schmittgen TD (2001) Analysis of relative gene expression data using real-time quantitative PCR and the 2^{(-Delta Delta C(T))} method. *Methods* **25**: 402–408.
- Lowry OH, Rosebrough NJ, Farr AL, and Randall RJ (1951) Protein measurement with the Folin phenol reagent. *J Biol Chem* **193**:265–275.
- Maayah ZH and El-Kadi AO (2016a) 5-, 12- and 15-Hydroxyeicosatetraenoic acids induce cellular hypertrophy in the human ventricular cardiomyocyte, RL-14 cell line, through MAPK- and NF-κB-dependent mechanism. *Arch Toxicol* **90**:359–373.
- Maayah ZH and El-Kadi AO (2016b) The role of mid-chain hydroxyeicosatetraenoic acids in the pathogenesis of hypertension and cardiac hypertrophy. *Arch Toxicol* **90**:119–136.
- Maayah ZH, Abdelhamid G, and El-Kadi AO (2015) Development of cellular hypertrophy by 8-hydroxyeicosatetraenoic acid in the human ventricular cardiomyocyte, RL-14 cell line, is implicated by MAPK and NF-κB. *Cell Biol Toxicol* **31**:241–259.
- Maayah ZH, Althurwi HN, Abdelhamid G, Lesyk G, Jurasz P, and El-Kadi AO (2016) CYP1B1 inhibition attenuates doxorubicin-induced cardiotoxicity through a mid-chain HETEs-dependent mechanism. *Pharmacol Res* **105**:28–43.
- Maayah ZH, Althurwi HN, El-Sherbeni AA, Abdelhamid G, Siraki AG, and El-Kadi AO (2017) The role of cytochrome P450 1B1 and its associated mid-chain hydroxyeicosatetraenoic acid metabolites in the development of cardiac hypertrophy induced by isoproterenol. *Mol Cell Biochem* **429**:151–165.
- Maayah ZH, Levasseur J, Siva Piragassam R, Abdelhamid G, Dyck JRB, Fahlman RP, Siraki AG, and El-Kadi AOS (2018) 2-Methoxyestradiol protects against pressure overload-induced left ventricular hypertrophy. *Sci Rep* **8**:2780.

- Matsumura N, Takahara S, Maayah ZH, Parajuli N, Byrne NJ, Shoieb SM, Soltys CM, Beker DL, Masson G, El-Kadi AOS, et al (2018) Resveratrol improves cardiac function and exercise performance in MI-induced heart failure through the inhibition of cardiotoxic HETE metabolites. *J Mol Cell Cardiol* **125**:162–173.
- Meng Q, Guo Y, Zhang D, Zhang Q, Li Y, and Bian H (2020) Tongsaimai reverses the hypertension and left ventricular remodeling caused by abdominal aortic constriction in rats. *J Ethnopharmacol* **246**:112154.
- Mosca L, Barrett-Connor E, and Wenger NK (2011) Sex/gender differences in cardiovascular disease prevention: what a difference a decade makes. *Circulation* **124**:2145–2154.
- Nakamura M and Sadoshima J (2018) Mechanisms of physiological and pathological cardiac hypertrophy. *Nat Rev Cardiol* **15**:387–407.
- Pascale JV, Lucchesi PA, and Garcia V (2021) Unraveling the role of 12- and 20- HETE in cardiac pathophysiology: G-protein-coupled receptors, pharmacological inhibitors, and transgenic approaches. *J Cardiovasc Pharmacol* **77**:707–717.
- Pedram A, Razandi M, Lubahn D, Liu J, Vannan M, and Levin ER (2008) Estrogen inhibits cardiac hypertrophy: role of estrogen receptor-beta to inhibit calcineurin. *Endocrinology* **149**:3361–3369.
- Petrov G, Regitz-Zagrosek V, Lehmkuhl E, Krabatsch T, Dunkel A, Dandel M, Dworatzek E, Mahmoodzadeh S, Schubert C, Becher E, et al (2010) Regression of myocardial hypertrophy after aortic valve replacement: faster in women? *Circulation* **122**(11 Suppl):S23–S28.
- Regitz-Zagrosek V and Kararigas G (2017) Mechanistic pathways of sex differences in cardiovascular disease. *Physiol Rev* **97**:1–37.
- Rocic P and Schwartzman ML (2018) 20-HETE in the regulation of vascular and cardiac function. *Pharmacol Ther* **192**:74–87.
- Rosano GM, Vitale C, Marazzi G, and Volterrani M (2007) Menopause and cardiovascular disease: the evidence. *Climacteric* **10**(10 Suppl):19–24.
- Ruppert M, Korkmaz-Icöz S, Loganathan S, Jiang W, Lehmann L, Oláh A, Sayour AA, Barta BA, Merkely B, Karcó M, et al (2018) Pressure-volume analysis reveals characteristic sex-related differences in cardiac function in a rat model of aortic banding-induced myocardial hypertrophy. *Am J Physiol Heart Circ Physiol* **315**:H502–H511.
- Salehiyeh S, Alborzi N, Azizian H, Esmailidehaj M, Hafizi Barjin Z, and Safari F (2024) Sex-related differences in hypertrophy response and cardiac expression of G protein-coupled estrogen receptor in rats with pressure overload. *Gene* **928**:148769.
- Sedláková L, Kikerlová S, Husková Z, Červenková L, Chábová V, Zicha J, Falck JR, Imig JD, Kompanowska-Jezierska E, Sadowski J, et al (2018) 20-Hydroxyeicosatetraenoic acid antagonist attenuates the development of malignant hypertension and reverses it once established: a study in Cyp1a1-Ren-2 transgenic rats. *Biosci Rep* **38**:BSR20171496.
- Shahim B, Kapelios CJ, Savarese G, and Lund LH (2023) Global public health burden of heart failure: an updated review. *Card Fail Rev* **9**:e11.
- Shimizu I and Minamino T (2016) Physiological and pathological cardiac hypertrophy. *J Mol Cell Cardiol* **97**:245–262.
- Shoieb SM and El-Kadi AOS (2018) S-Enantiomer of 19-hydroxyeicosatetraenoic acid preferentially protects against angiotensin II-induced cardiac hypertrophy. *Drug Metab Dispos* **46**:1157–1168.
- Shoieb SM and El-Kadi AOS (2020) Resveratrol attenuates angiotensin II-induced cellular hypertrophy through the inhibition of CYP1B1 and the cardiotoxic mid-chain HETE metabolites. *Mol Cell Biochem* **471**:165–176.
- Shoieb SM, Alammari AH, Levasseur J, Silver H, Dyck JRB, and El-Kadi AOS (2022) Ameliorative role of fluconazole against abdominal aortic constriction-induced cardiac hypertrophy in rats. *J Cardiovasc Pharmacol* **79**:833–845.
- Skavdahl M, Steenbergen C, Clark J, Myers P, Demianenko T, Mao L, Rockman HA, Korach KS, and Murphy E (2005) Estrogen receptor-beta mediates male-female differences in the development of pressure overload hypertrophy. *Am J Physiol Heart Circ Physiol* **288**:H469–H476.
- Spector AA (2009) Arachidonic acid cytochrome P450 epoxygenase pathway. *J Lipid Res* **50**:S52–S56.
- Tang F, Lu M, Yu L, Wang Q, Mei M, Xu C, Han R, Hu J, Wang H, and Zhang Y (2016) Inhibition of TNF- α -mediated NF- κ B activation by ginsenoside Rg1 contributes the attenuation of cardiac hypertrophy induced by abdominal aorta coarctation. *J Cardiovasc Pharmacol* **68**:257–264.
- Tran DT, Ohinmaa A, Thanh NX, Howlett JG, Ezekowitz JA, McAlister FA, and Kaul P (2016) The current and future financial burden of hospital admissions for heart failure in Canada: a cost analysis. *CMAJ Open* **4**:E365–E370.
- Tse MM, Aboutabl ME, Althurwi HN, Elshenawy OH, Abdelhamid G, and El-Kadi AO (2013) Cytochrome P450 epoxygenase metabolite, 14,15-EET, protects against isoproterenol-induced cellular hypertrophy in H9c2 rat cell line. *Vascul Pharmacol* **58**:363–373.
- Waldman M, Peterson SJ, Arad M, and Hochhauser E (2016) The role of 20-HETE in cardiovascular diseases and its risk factors. *Prostaglandins Other Lipid Mediat* **125**:108–117.
- Westphal C, Konkel A, and Schunck WH (2015) Cytochrome p450 enzymes in the bioactivation of polyunsaturated fatty acids and their role in cardiovascular disease. *Adv Exp Med Biol* **851**:151–187.
- Yang L, Mäki-Petäjä K, Cheriyan J, McEniery C, and Wilkinson IB (2015) The role of epoxyeicosatrienoic acids in the cardiovascular system. *Br J Clin Pharmacol* **80**:28–44.
- Zhang M, Shu H, Chen C, He Z, Zhou Z, and Wang DW (2022) Epoxyeicosatrienoic acid: a potential therapeutic target of heart failure with preserved ejection fraction. *Biomed Pharmacother* **153**:113326.
- Zordoky BN, Aboutabl ME, and El-Kadi AO (2008) Modulation of cytochrome P450 gene expression and arachidonic acid metabolism during isoproterenol-induced cardiac hypertrophy in rats. *Drug Metab Dispos* **36**:2277–2286.
- Zordoky BN and El-Kadi AO (2008) Modulation of cardiac and hepatic cytochrome P450 enzymes during heart failure. *Curr Drug Metab* **9**:122–128.